JCTC Journal of Chemical Theory and Computation

Article

pubs.acs.org/JCTC

Improved Angle Potentials for Coarse-Grained Molecular Dynamics Simulations

Monica Bulacu,*[,†] Nicolae Goga,[†,‡] Wei Zhao,[§] Giulia Rossi,[∥] Luca Monticelli,[⊥,∥] Xavier Periole,[†,§] D. Peter Tieleman,*[,§] and Siewert J. Marrink*[,†]

[†]Groningen Biomolecular Sciences and Biotechnology Institute and Zernike Institute for Advanced Materials, University of Groningen, Nijenborgh 7, 9747 AG Groningen, The Netherlands

[‡]FILS, Politechnica University of Bucharest, Splaiul Independentei 313, Bucharest, Romania

[§]Department of Biological Sciences and Institute for Biocomplexity and Informatics, University of Calgary, 2500 University Drive NW, Calgary, AB, Canada T2N 1N4

[∥]INSERM, UMR-S665, Paris, F-75015, France, and

[⊥]INTS, Paris, France

ABSTRACT: Potentials routinely used in atomistic molecular dynamics simulations are not always suitable for modeling systems at coarse-grained resolution. For example, in the calculation of traditional torsion angle potentials, numerical instability is often encountered in the case of very flexible molecules. To improve the stability and accuracy of coarse-grained molecular dynamics simulations, we propose two approaches. The first makes use of improved forms for the angle potentials: the restricted bending (ReB) potential prevents torsion angles from visiting unstable or unphysical configurations and the combined bending-torsion (CBT) potential smoothly flattens the interactions when such configurations are sampled. In the second approach, dummy-assisted dihedral (DAD), the torsion potential is applied differently: instead of acting directly on the beads, it acts on virtual beads, bound to the real ones. For simple geometrical reasons, the unstable region is excluded from the accessible conformational space. The benefits of the new approaches are demonstrated in simulations of polyethylene glycol (PEG), polystyrene (PS), and polypeptide molecules described by the MARTINI coarse-grained force field. The new potentials are implemented in an *in-house* version of the Gromacs package, publicly available.

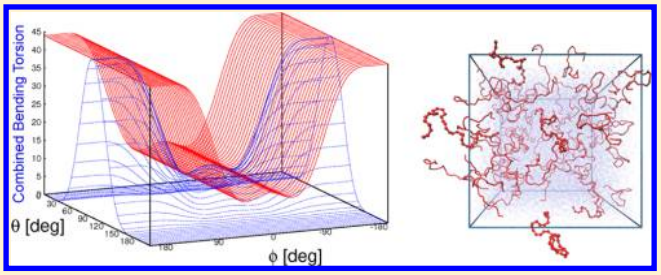

INTRODUCTION

Molecular Dynamics (MD) is a computational method that simulates the structure and dynamic behavior of matter by using a discrete representation of particles, interacting with each other. The equations of motion for all the particles are integrated numerically, in a sequence of successive time intervals such that particle trajectories are obtained in a period of time. Besides direct observation of the occurring phenomena at the atomistic level, the macroscopic properties of the simulated systems are also accessible by applying statistical analysis on the generated ensemble of configurations.

The core of a MD program is the force calculation followed by the integration of the equations of motion. The most computationally demanding forces are the nonbonded interactions acting between dynamically formed pairs of particles (electrostatic and van der Waals interactions). The bonded forces model the chemical bonds in a molecule (bond, bending angle and dihedral angle interactions), which are of essential importance in obtaining a valid molecular structure and the correct macroscopic behavior. Typical bonded potentials have simplified forms (often harmonic and other idealized expressions) and are robust and reliable for traditional atomistic simulations, when a time step restricted to a few femtoseconds is used.

However, due to the upcoming field of coarse-grained (CG) simulations, these potentials start to show some limitations. In CG models the atomistic particles are replaced by a reduced number of beads that are small enough to keep the desired chemical detail but big enough to reduce significantly the total number of particles. The effective interacting potentials between the new CG beads are softer than the atomistic ones, so that larger integration time steps can be used. In a growing number of cases, the combination of larger time steps with an increased molecular flexibility leads inevitably to singularities, in particular in the bonded potentials. Hence, the need for revising the bonded potentials is obvious for coarse-grained MD simulations to fully and reliably use the outstanding computational resources available nowadays.

In this paper, we address this challenge and we start improving the angle interactions, by proposing novel angular potentials and by modifying the action of the torsion potential.

Received: March 19, 2013
Published: June 18, 2013

Our functional forms for these interactions are described and tested in MD simulations of both polymers and proteins, using the CG MARTINI model.[1,2]

THEORY

Standard Angle Potentials. Figure 1 illustrates a simple linear molecule with the bonds and bending and torsion angles characterizing its structure.

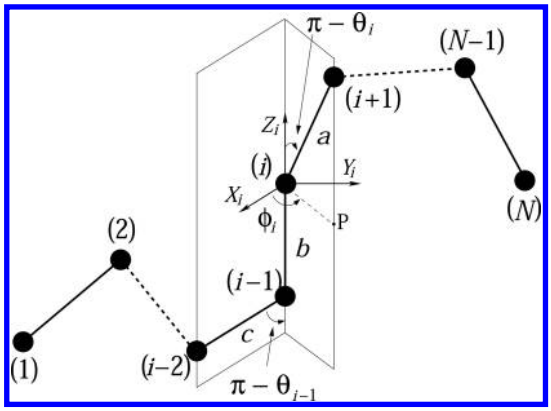

Figure 1. Schematic representation of a simple linear molecule. Monomer indices are indicated in parentheses. *a*, *b*, and *c* are three selected bonds, θ are the bending angles, and ϕ is the dihedral angle. *P* is the projection of the bead $i + 1$ on the X_iY_i plane and allows for a better visualization of the torsion angle ϕ_i.

The bending angle θ_i is created by two successive bond vectors, named *a* and *b* in Figure 1:

$$\cos\theta_i = \frac{\vec{a}\cdot\vec{b}}{\|\vec{a}\|\|\vec{b}\|} \tag{1}$$

and the torsion angle ϕ_i is the angle between two planes (one defined by *a* and *b* bonds and the other by *b* and *c*). The term *torsion* is often used interchangeably with the term *dihedral* when referring to both the angle and its associated potential. The dihedral angle can be calculated as the angle between the unit normals of the two planes ($\vec{u} = \vec{a} \times \vec{b}$ and $\vec{v} = \vec{b} \times \vec{c}$) or as the angle between two vectors lying in each of the planes. In both cases, the same formula is derived:[3,4]

$$\cos\phi_i = \frac{\vec{u}\cdot\vec{v}}{\|\vec{u}\|\|\vec{v}\|} = \frac{(\vec{a}\cdot\vec{b})(\vec{b}\cdot\vec{c}) - (\vec{a}\cdot\vec{c})(\vec{b}\cdot\vec{b})}{\|a\|\|b\|^2\|c\|\sin\theta_{i-1}\sin\theta_i} \tag{2}$$

It is evident that ϕ_i becomes geometrically undefined when at least one of the bending angles from the bead quadruplet is equal to 0° or 180°. To establish the quadrant of ϕ_i, either the $sign(\phi_i) = (\vec{a} \times \vec{b})\cdot\vec{c}$ or sin ϕ_i are evaluated. If *sign* is negative (sin $\phi_i < 1$), the dihedral angle is considered negative: $\phi_i = 0° - \phi_i$ (in IUPAC convention) or $\phi_i = 360° - \phi_i$ (in polymer convention). In this paper, we make use of the IUPAC convention[5] for the dihedral angle definition for both biological and polymeric systems. In this way, our results will be presented in an unitary manner and be consistent with the Gromacs[6] and VMD[7] style.

The most common bending potentials V_B used in MD simulations are harmonic in θ:

$$V_B(\theta_i) = \frac{1}{2}k_\theta(\theta_i - \theta_0)^2 \tag{3}$$

or in cos θ (cosine harmonic—CH):

$$V_B(\theta_i) = \frac{1}{2}k_\theta(\cos\theta_i - \cos\theta_0)^2 \tag{4}$$

with θ_0 the reference value of the bending angle and k_θ the bending constant. The graphical representation of these two bending potentials is given in Figure 2.

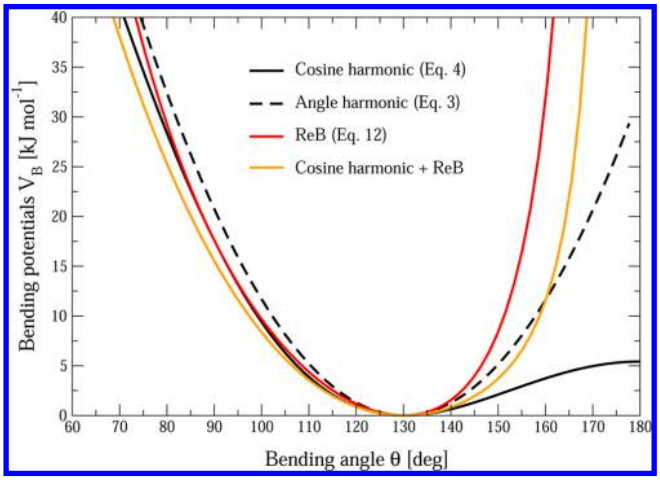

Figure 2. Bending angle potentials: cosine harmonic (solid black line), angle harmonic (dashed black line), and restricted bending (red) with the same bending constant k_θ = 85 kJ mol^{-1} and equilibrium angle θ_0 = 130°. The orange line represents the sum of a cosine harmonic (k_θ = 50 kJ mol^{-1}) with a restricted bending (k_θ = 25 kJ mol^{-1}) potential, both with θ_0 = 130°.

The bending forces acting on the three beads forming the θ_i angle ($k = i - 1, i, i + 1$) are calculated as

$$F_B^k(\theta_i) = -\nabla_k V_B(\theta_i) = -\frac{\partial V_B(\theta_i)}{\partial \vec{r}_k} \tag{5}$$

where, for the derivative, two chain rules are traditionally used: $(dV_B/d\theta_i)(d\theta_i/d\cos\theta_i)(\partial\cos\theta_i/\partial\vec{r}_k)$ for eq 3 and $(dV_B/d\cos\theta_i)(\partial\cos\theta_i/\partial\vec{r}_k)$ for eq 4. In the first case, a singularity for θ = 0° and θ = 180° appears, since $d\theta_i/d\cos\theta_i = 1/\sin\theta_i$.

The derivative of the bending angle with respect to the particle vector is calculated as

$$\frac{\partial\cos\theta_i}{\partial\vec{r}_k} = \frac{1}{\|\vec{a}\|\|\vec{b}\|}\frac{\partial}{\partial\vec{r}_k}(\vec{a}\cdot\vec{b}) - \frac{\cos\theta_i}{2}\left[\frac{1}{\|\vec{a}\|^2}\frac{\partial}{\partial\vec{r}_k}\|\vec{a}\|^2 + \frac{1}{\|\vec{b}\|^2}\frac{\partial}{\partial\vec{r}_k}\|\vec{b}\|^2\right] \tag{6}$$

For the torsion potential, V_T, three expressions are mostly used (see Figure 3). The angle harmonic potential is given by

$$V_T(\phi_i) = \frac{1}{2}k_\phi(\phi_i - \phi_0)^2 \tag{7}$$

with k_ϕ the force constant and ϕ_0 the equilibrium angle. The periodic cosine (PC) potential,

$$V_T(\phi_i) = k_\phi[1 + \cos(m\phi_i - \delta)] \tag{8}$$

gives one or more maxima (depending on the multiplicity *m*) at δ/m, with the periodicity of $360°/m$. This potential is traditionally used for proper dihedrals in biological systems (e.g., proteins). By summing up a set of such torsion potentials (each with its torsion constant k_ϕ, angle δ and multiplicity *m*),

dx.doi.org/10.1021/ct400219n | J. Chem. Theory Comput. 2013, 9, 3282−3292

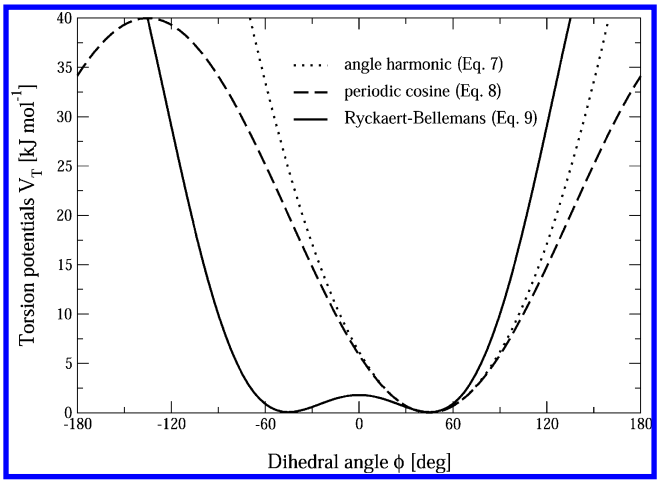

Figure 3. Torsion potentials with the same torsion constant $k_\phi = 20$ and equilibrium angle $\phi_0 = 45°$: angle harmonic (dotted line), periodic cosine with multiplicity 1 (dashed line) and Ryckaert−Bellemans with coefficients $a_0 = 0.5$, $a_1 = -1.41$, $a_2 = 1$, and $a_3 = a_4 = a_5 = 0$ (solid).

specific energy landscapes for the torsion interaction can be obtained.

The third torsion potential commonly used is the cosine polynomial (solid line in Figure 3)

$$V_T(\phi_i) = k_\phi \sum_{n=0}^{p} a_n \cos^n \phi_i \tag{9}$$

introduced by Ryckaert and Bellemans[8] (RB) with $p = 5$ for alkanes. This form can mimic different dihedral potentials by adjusting the constant parameters a_n. Unlike the previous potentials (eq 7 and eq 8), these are symmetrical around 0°. For example, with $p = 2$ and a_n coefficients related with a reference angle ϕ_0, this potential is equivalent with a cosine harmonic potential described by eq 4, with two maxima at $\pm\phi_0$. Power series in cos ϕ up to the third power ($p = 3$ in eq 9) are also very frequently used.[9,10] The transfer between the polymer and IUPAC conventions for the dihedral angles, is done by applying a $(-1)^n$ factor to each of the a_n parameters.

The force arising from the dihedral potential acts on all four particles defining the dihedral angle ϕ_i:

$$F_T^l(\phi_i) = -\nabla_l V_T(\phi_i) = -\frac{\partial V_T(\phi_i)}{\partial \vec{r}_l} \tag{10}$$

with l being $i - 2$, $i - 1$, i or $i + 1$.

As for the bending potential, the gradient $\nabla_l V_T(\phi_i)$ is obtained using the following chain rule factorization, $\partial V_T/\partial \vec{r}_l = (dV_T/d\phi_i)(d\phi_i/(d\cos\ \phi_i)(\partial \cos\ \phi_i/\partial \vec{r}_l)$, which leads to a singularity for $\phi = 0°$ and $\phi = 180°$ because $d\phi/d\cos\ \phi = -1/\sin\ \phi$. In the case of torsion potentials described as powers of cos ϕ, this singularity can be avoided by changing the chain rule to $\partial V_T/\partial \vec{r}_l = (dV_T/d\cos\ \phi_i)(\partial \cos\ \phi_i/\partial \vec{r}_l)$.

The derivative of the dihedral angle with respect to the Cartesian coordinates is then calculated as

$$\frac{\partial \cos\ \phi_i}{\partial \vec{r}_l} = \frac{1}{\|\vec{u}\|\|\vec{v}\|}\frac{\partial}{\partial \vec{r}_l}(\vec{u}\cdot\vec{v}) - \frac{\cos\ \phi_i}{2}\left[\frac{1}{\|\vec{u}\|^2}\frac{\partial}{\partial \vec{r}_l}\|\vec{u}\|^2 + \frac{1}{\|\vec{v}\|^2}\frac{\partial}{\partial \vec{r}_l}\|\vec{v}\|^2\right] \tag{11}$$

After replacing the norms in eq 11, the derivative becomes a sum of terms, each containing the factor $1/(\sin^\alpha \theta_i \sin^\beta \theta_{i-1})$ with α and β being 1, 2, or maximum 3.

The computed bending and torsion forces are added to the total force per particle and the integration of motion produces new coordinates (new angles). This iteration process may be interrupted when one of the formulas involved in the calculus leads to numerical instability (division by zero). For the angle potentials described in this section such situation can occur in three cases:

1. the calculation of the torsion angle (eq 2): if one of the sin terms from the denominator is identically zero the cos ϕ cannot be calculated (i.e., $\theta = 0°$, 180°).
2. the derivative of the angles (θ or ϕ) with respect to their cosine leads to a $1/\sin\ \theta$ and $1/\sin\ \phi$ singularity for θ or $\phi = 0°$, 180° in the bending and torsion force, respectively.
3. the derivative of the dihedral angle ϕ with respect to the Cartesian variables (eq 11) leads to $1/\sin\ \theta$, $1/\sin^2\ \theta$ and $1/\sin^3\ \theta$ singularities for θ_i or $\theta_{i-1} = 0°$, 180° in the expression of the force.

The situation of $\theta = 0°$ is, in fact, impossible when a Lennard-Jones potential is used between second neighbor beads and it does not allow two beads to overlap. This is also the reason that prevents the cancellation of the norms of the bonds (both in eq 1 and eq 2). The situations of $\theta = 180°$, $\phi = 0°$, or $\phi = 180°$ are considered as "rare events" for atomistic simulations and, most of the time, are ignored or treated superficially. When encountered, in practice, a restart from the last frame (check point) saved before the crash is often sufficient to explore a different configuration without singularities. In coarse-grained MD simulations, however, the angle potentials are softer and these events are more frequent. A more careful treatment is required to allow for high-throughput. We follow two approaches: the use of improved angle potentials and the use of dummy assisted dihedrals.

Improved Angle Potentials. This subsection describes two angle potentials modified in such way to eliminate the numerical singularities described above. The first one, the restricted bending (ReB) potential, prevents the bending angles θ_{i-1} and θ_i, forming the dihedral, from reaching the 180° value. The second one, the combined bending-torsion (CBT) potential, disregards any effects of the dihedral becoming ill-defined, keeping the dihedral force and potential calculation continuous in entire angle range.

ReB Potential. To systematically hinder the bending angles from reaching the 180° value, we propose a very simple solution: the modification of the bending potential itself. This is done by dividing the eq 4 by a $\sin^2\ \theta$ factor:

$$V_{ReB}(\theta_i) = \frac{1}{2}k_\theta \frac{(\cos\ \theta_i - \cos\ \theta_0)^2}{\sin^2\ \theta_i} \tag{12}$$

Figure 2 shows the comparison between the introduced potential, eq 12, with the standard ones (eqs 3 and 4).

The wall of the ReB potential is very repulsive in the region close to 180°, and as a result, the bending angles are kept within a "safe" interval, far from instabilities. The power 2 of $\sin\ \theta_i$ at the denominator has been chosen to guarantee this behavior and allows an elegant differentiation:

$$F_{\mathrm{ReB}}(\theta_i) = \frac{2k_\theta}{\sin^4\theta_i}(\cos\theta_i - \cos\theta_0)(1 - \cos\theta_i\cos\theta_0)\frac{\partial\cos\theta_i}{\partial\vec{r}_k} \quad (13)$$

Due to its construction, the restricted bending potential cannot be used for equilibrium θ_0 values too close to 0° or 180° (from our experience, at least 10° difference is recommended). Also, note that, in the starting configuration, all the bending angles have to be in the "safe" interval to avoid initial instabilities.

This novel bending potential can be used in combination with any form of torsion potential, and it will avoid the singularities caused by the beads alignment. It can be also added to a "standard" bending potential to affect the angle around 180° but to keep its original form around the minimum (see the green curve in Figure 2).

In a manner very similar to the restricted bending potential, a restricted torsion can be introduced:

$$V_{\mathrm{ReT}}(\phi_i) = \frac{1}{2}k_\phi\frac{(\cos\phi_i - \cos\phi_0)^2}{\sin^2\phi_i} \quad (14)$$

with the advantages of being a function of cos ϕ (no derivation problems in sin ϕ) and of keeping the torsion angle at only one minimum value. In this case, the factor $\sin^2\phi$ does not allow the dihedral angle to move from the [−180°:0] to [0:180°] interval, that is, not to have both $-\phi_0$ and $+\phi_0$ maxima, but only one of them. Note that this is equivalent to a harmonic potential.

CBT Potential. The second method consists of coupling the torsion potential (in a cosine form) with the bending potentials of the adjacent bending angles in a unique expression:

$$V_{\mathrm{CBT}}(\theta_{i-1}, \theta_i, \phi_i) = k_\phi \sin^3\theta_{i-1}\sin^3\theta_i\sum_{n=0}^{4} a_n\cos^n\phi_i \quad (15)$$

The CBT potential has already been proposed by Bulacu and Van der Giessen[11] for polymer melt simulations and has been successfully used in a number of subsequent simulations of polymeric materials.[12−15]

This potential has two main advantages:

- It does not only depend on the dihedral angle ϕ_i (between the $i-2$, $i-1$, i, and $i+1$ beads) but also on the bending angles θ_{i-1} and θ_i formed by three adjacent beads ($i-2$, $i-1$ and i, and $i-1$, i, and $i+1$, respectively). The two $\sin^3\theta$ prefactors, tentatively suggested by Scott and Scheraga[16] and theoretically discussed by Pauling,[17] cancel the torsion potential and force when either of the two bending angles approaches the value of 180°.
- Its dependence on ϕ_i is expressed through a polynomial in cos ϕ_i that avoids the singularities in ϕ = 0° or 180° in the torsional force calculus.

These two important properties make the CBT potential well-behaved for MD simulations with weak constraints on the bending angles or even for steered/nonequilibrium MD in which the bending and torsion angles suffer major modifications. When using the CBT potential, the bending potentials for the adjacent θ_{i-1} and θ_i may have any form. It may be also possible to leave θ_{i-1} and θ_i angles free. Figure 4 illustrates the difference between a torsion potential with and without the $\sin^3\theta$ factors (blue and gray curves, respectively).

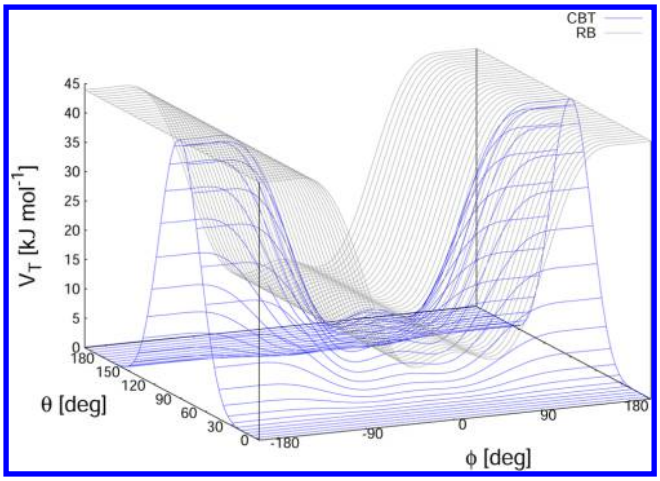

Figure 4. In blue, surface plot of the combined bending−torsion potential (eq 15 with k_ϕ = 10 kJ mol^{-1}, a_0 = 2.41, a_1 = −2.95, a_2 = 0.36, a_3 = 1.33) when, for simplicity, the bending angles behave the same ($\theta_1 = \theta_2 = \theta$); in gray, the same torsion potential without the $\sin^3\theta$ terms.

Additionally, the derivative of V_{CBT} with respect to the Cartesian variables is straightforward:

$$\frac{\partial V_{\mathrm{CBT}}(\theta_{i-1}, \theta_i, \phi_i)}{\partial\vec{r}_l} = \frac{\partial V_{\mathrm{CBT}}}{\partial\theta_{i-1}}\frac{\partial\theta_{i-1}}{\partial\vec{r}_l} + \frac{\partial V_{\mathrm{CBT}}}{\partial\theta_i}\frac{\partial\theta_i}{\partial\vec{r}_l} + \frac{\partial V_{\mathrm{CBT}}}{\partial\phi_i}\frac{\partial\phi_i}{\partial\vec{r}_l} \quad (16)$$

with the derivatives from all three terms already known from eq 6 and eq 11.

A very similar form with sin θ_{i-1} sin θ_i is used in a reactive force field for hydrocarbons by van Duin et al.[18] Nevertheless, in light of the derivation from eq 11, only third-power sine terms ensure the numerical stability.

Based on a cosine form without multiplicity, the CBT can only be symmetrical around 0°. To obtain an asymmetrical dihedral angle distribution (e.g., only one maximum in [−180°:180°] interval), a "standard" torsion potential such as eq 7 or eq 8 should be used. However, these two forms have the inconveniences of the force derivation (1/sin ϕ) and of the beads alignment (θ_i or θ_{i-1} = 0°, 180°). Coupling such non-cos ϕ potentials with $\sin^3\theta$ factors does not improve simulation stability, since there are cases in which θ and ϕ are simultaneously 180°. The integration at this step would be possible (due to the canceling of the torsion potential) but the next step would be singular (θ is not 180° and ϕ is very close to 180°).

Dummy-Assisted Dihedrals. This subsection describes the dummy-assisted dihedral (DAD) method that avoids the numerical instabilities by changing the way in which the angle potentials are applied. In DAD, the dihedral angle is defined by extra beads (dummies) instead of conventional particles. The schematic in Figure 5 illustrates the definition of the additional particles (type D) based on the original ones (type B). Each dummy particle D_i is constrained at a distance d from B_i, in the plane defined by B_{i-1}, B_i, and B_{i+1}, maximizing its distance to B_{i-1} and B_{i+1} and with equal angles $B_{i-1}B_iD_i$ and $D_iB_iB_{i+1}$. The

dx.doi.org/10.1021/ct400219n | J. Chem. Theory Comput. 2013, 9, 3282−3292

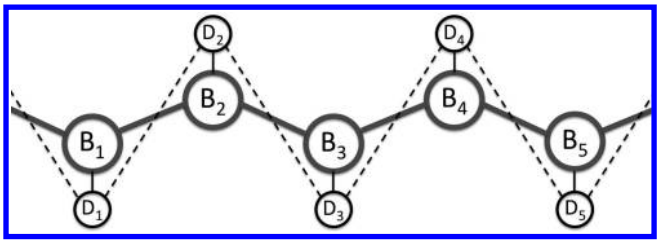

Figure 5. Schematic of the dummy assisted dihedral (DAD) potential. B_i are the initial particles and D_i the associated dummies. The dummy particles are constraint at a fixed distance from the original particles and the angles $B_{i-1}B_iD_i$ and $D_iB_iB_{i+1}$ are subjected to a harmonic potential with an equilibrium angle complementing the $B_{i-1}B_iB_{i+1}$ value to 360°. A torsion potential D−D−D−D replaces the original B−B−B−B potential. Associated parameters are given in Table 1.

use of D_{1-4} particles instead of B_{1-4} resolves the instability of the B_{1-4} dihedral resulting from the exploration of values close to 180° by the $B_{i-1}B_iB_{i+1}$ angles where i = 2 and 3. For simple geometrical considerations, the angles $D_{i-1}D_iD_{i+1}$ are unlikely to explore values close to 180°; this would imply an extremely large enthalpic penalty. In principle, DAD can be applied on any type of molecule after a quick calibration of the corresponding parameters. The parameters associated with its use to replace the conventional dihedral potential that describes the protein backbone in the MARTINI coarse grained force field[19,20] are listed in Table 1. Dummy particles D_i are

Table 1. Parameters of the Dummy-Assisted Dihedral for the MARTINI Protein Force Field[a]

bonded term	SS	reference value [nm or degree]	k [kJ mol^{-1}]	m
$d(B_iD_i)$	all	0.15	constraint	
$B_{i-1}B_iD_i$, $D_iB_iB_{i+1}$	helix	132 (96)	100	
	coil	116.5 (127)	100	
	extended	113 (134)	100	
	turn	130 (100)	100	
$D_{i-1}D_iD_{i+1}D_{i+2}$	helix	−142.7	400	1
	coil	16.4	3.47	1
		−70	0.96	2
	extended	27	10/25/40	1
	turn	−155.0	2.64	1
		−88.5	1.04	2
		−82.7	1.05	3
		116.65	0.68	4
		−103.7	1.02	5
	bend	−126.5	1.09	1
		−58	0.99	2

[a]SS designates the secondary structure type; reference values for the distance, bond and dihedral angle potentials, force constant (k), and multiplicity (m, when relevant) are given. The actual target value for the bond angles (cosine potential) are different from the reference value and are given in parentheses. The definition of the particles, bending and torsion angles is shown in Figure 5.

constraint at a 0.15 nm distance from the backbone bead B_i, and they satisfy $B_{i-1}B_iD_i = D_iB_iB_{i+1} = (360° - B_{i-1}B_iB_{i+1})/2$. The angle $B_{i-1}B_iB_{i+1}$ is already defined by the MARTINI force field. This definition maintains D_i in line with the normal to the direction defined by B_{i-1} and B_{i+1}. A torsion potential D−D−D−D replaces the original B−B−B−B potential. In Table 1, we give the parameters for each of the secondary structure types according to the MARTINI force field definition of the backbone bonded terms. These parameters were obtained using the following steps: (i) backbone dihedral angle distributions were extracted from a database of protein structures as done previously,[19] (ii) an initial set of potentials were obtained by operating a simple Boltzmann inversion of the distributions and fitting the results using a linear combination of periodic cosine potentials (eq 8); (iii) finally, the parameters (Table 1) were tuned manually to reach a good match of the dihedral distributions obtained from the protein database in CG MD simulations. Note, however, that it is only on the extended secondary structure type that the use of DAD would actually be required. The general procedure for parametrization has been described in detail elsewhere.[1,19] The remainder of the bonded and nonbonded parameters does not require any change from the original MARTINI force field. The mass of the bead B_i is shared with D_i, 36 amu each, and D particles do not have any nonbonded interactions with the other particles.

IMPLEMENTATION

The angle potentials proposed here—ReB and CBT—have been implemented into an *in-house* version of Gromacs, publicly available on the MARTINI web-page (http://cgmartini.nl).

Table 2 shows the three potentials with the corresponding input parameters needed in the topology files (.itp) describing

Table 2. Gromacs Definitions of the Intramolecular Interaction Concerning the Modified Potentials[a]

interaction type	directive	# at.	ftp	param.
ReB	angles	3	10	θ_0, k_θ
ReT	dihedrals	4	10	ϕ_0, k_ϕ
CBT	dihedrals	4	11	k_ϕ, a_0, a_1, a_2, a_3, a_4

[a]The function type and parameters conform with the Gromacs definition.

the molecular interactions. Extra subroutines have been included into the original Gromacs "bondfree.c" subroutine to calculate the dihedral angle (its cosine and the contributions of the torsion force on each particle forming the dihedral). The angle is computed using the *dot-product* method and the forces following the approach of Allen and Tildesley.[21] The ReB subroutine is very similar to the one for the harmonic bending calculation. Only a new derivative is implemented (eq 13). In the CBT subroutine, when a θ angle is 180° its sine is made artificially a very small number and the force and potential calculation may continue. Their values will cancel due to the $\sin^3\theta$ terms. This cancellation is continuous, avoiding steps in the potential and force.

Additionally, the *input−output* and the preprocessing subroutines have been modified to read/write the new molecular topology files and to create the binary topology file (.tpr) for the MD run. The utilities *mk_angndx* and *g_angle* have been also extended to describe and calculate the new types of angles.

The DAD method operates with any torsion potentials and does not require code modifications. However, a redefinition of the interacting beads and reference angle is necessary. The use of the DAD potential with the MARTINI CG force field is supported by a script available on the MARTINI web-page.

APPLICATIONS

Coarse-Grained Simulations of Polymers. The advantages of the newly implemented potentials are shown in coarse-grained simulations of polyethylene glycol (PEG) and polystyrene (PS).

Polyethylene Glycol (PEG). We have simulated an ensemble of polyethylene glycol (PEG) chains in water, at low density (Figure 6), using the PEG model based on the MARTINI force-field, developed by Lee et al.[22] We will call this original model the PEG-OR model. The polymer is represented as a linear chain of CG beads (as in Figure 1), each representing a C−O−C chemical moiety. Bonded interactions include bonds, bending and torsion angles along the backbone. In PEG-OR, a cosine-harmonic function (eq 4) is used for the bending potential, and a combination of four torsion potentials (eq 8) is used for the dihedral angle (see the parameters in Table 3).

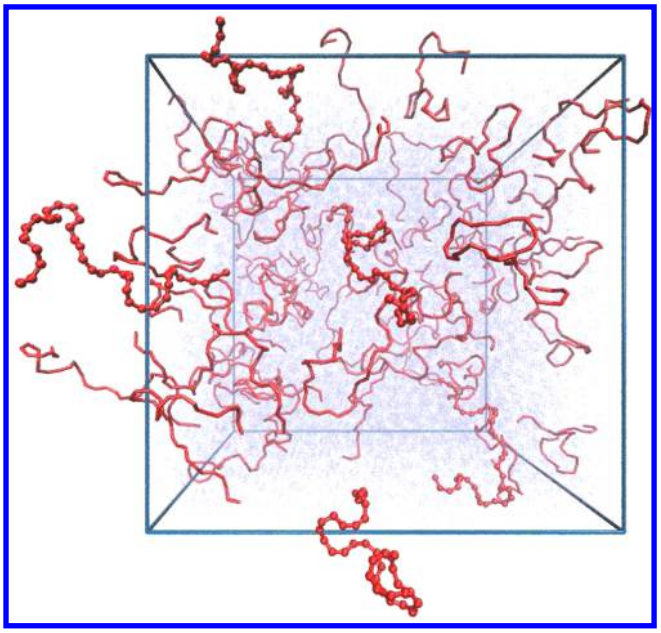

Figure 6. Snapshot from the simulation of an ensemble of PEG polymer chains in water. The polymer chains are depicted as red ropes and the water is shown as a blue haze. Some polymers are represented as linear chains of beads to show the coarse-grained model.

Table 3. Angle Potentials Used in the PEG Simulations: Type, Reference Angle, and Optimum Interaction Parameters

	bending			torsion			
	type	θ_0 [deg]	k_B [kJ mol^{-1}]	type	ϕ_0 [deg]	k_ϕ [kJ mol^{-1}]	m/ a_i
PEG-OR	CH	130	85	PC	180	1.96	1
				PC	0	0.18	2
				PC	0	0.33	3
				PC	0	0.12	4
PEG-ReB	CH	130	50	idem			
	ReB	130	25				
PEG-CBT	CH	116	110	CBT	k_ϕ = 10	a_0 = 2.41	
						a_1 = −2.95	
						a_2 = 0.36	
						a_3 = 1.33	
						a_4 = 0.00	

The model of Lee et al.[22] shows excellent agreement with atomistic simulation results for the bending and torsion angle distributions, and with experimental data for the chain size. To test the stability of the PEG-OR model, we have considered a system of 56 PEG polymer chains (each of 37 monomers) in water (13312 water coarse-grained particles) using the input files provided at http://cgmartini.nl and standard simulation conditions: T = 300 K (Berendsen thermostat), P = 1.0 atm (isotropic coupling), time step δt = 0.04 ps, and periodic boundary conditions. We performed 20 identical simulations starting with different seeds for the velocity generator. The average simulation time before a system became unstable was 5 ns and the maximum simulated time 15 ns. The model thus poses serious stability issues. A moderate improvement in stability was obtained by decreasing the time step to δt = 0.01 ps or by using an angle harmonic form (eq 3) for the bending potential with θ_0 = 130° and k_θ = 50 kJ mol^{-1} (as suggested on the MARTINI Web site).

The black curves in Figure 7 represent the probability distributions for the bending angle θ and dihedral angle ϕ obtained during the PEG-OR simulation. The histograms are calculated from all the angles along the polymer chain and for all the coordinate frames written out during the simulation. The distributions indicate that the bending angles close to 180° are sampled, causing the numerical instability as sin ϕ becomes undefined (eq 2). To avoid this instability we propose two new models using the improved potentials described:

- PEG-ReB, a model using the restricted bending potential for the bending angle and the same torsion potentials as in PEG-OR.
- PEG-CBT, a model using the same bending potential as in PEG-OR and the combined bending torsion potential for the dihedral (eq 15).

Table 3 includes all the parameters of these potentials. In the PEG-ReB and PEG-CBT simulations, the polymer's behavior is expected to remain unchanged since the modified angular potentials have almost the same form as the ones used in the PEG-OR simulation (only their analytical expression differs). The advantage of using the potentials introduced here is to improve the simulation stability at larger integration time steps and at higher temperatures.

For each of the two new models, three independent simulations have been performed starting with the same initial configuration and settings of those used for the PEG-OR model. When starting the PEG-ReB simulations, all the bending angles from the initial configuration have to be away from the θ = 180° to avoid the instabilities (in practice, a minimum difference of ≈10° suffices). This can be incorporated during the initial chain generation procedure or by performing a short MD run with a very small time step and a large force constant in a standard bending potential. After such proper setup, the simulations with restricted bending are stable on the time scale tested (up to tens of microseconds).

The ReB potential indeed prevents the bending angle from reaching values close to 180° (observe the difference between the black and the colored curves in Figure 7a). This effect is enhanced with increasing the bending force constant used for the restricted potential. However, the ReB modifies both the bending and the torsion angle distributions compared with the original ones, by changing their spread around the equilibrium values. For example, k_θ = 85 kJ mol^{-1} leads to a visible increase of the bending maxima, while a lower k_θ = 50 kJ mol^{-1} allows

dx.doi.org/10.1021/ct400219n | J. Chem. Theory Comput. 2013, 9, 3282−3292

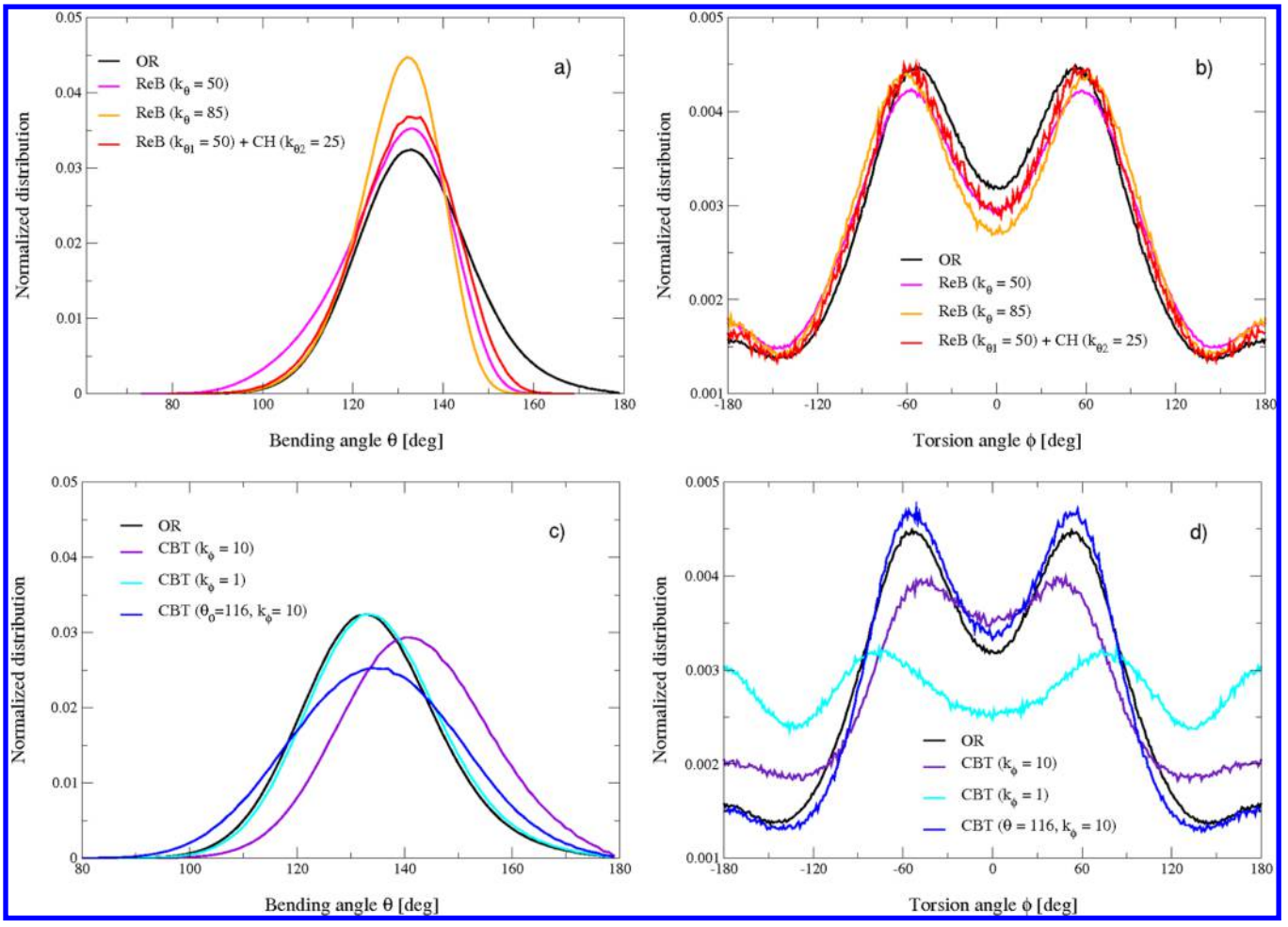

Figure 7. Probability distributions of the bending angle θ and the dihedral angle ϕ obtained during the simulations. The histograms obtained using the PEG-OR model are compared with PEG-ReB (a and b) and PEG-CBT (c and d) models described in the text. The force constants referred in the figure are given in kJ mol^{-1} units.

the sampling of smaller bending angles. These modifications entail the unwanted alteration of the torsion angle distribution and, consequently, of the end-to-end distance of the polymer chain. To minimize these effects, we propose to use the sum of two expressions for the bending potential: the original cosine-type potential (θ_0 = 130° and k_θ = 50 kJ mol^{-1}) combined with the ReB potential (θ_0 = 130° and k_θ = 25 kJ mol^{-1}). The cosine-type enforces the correct distribution and the restricted type removes the accessibility to 180° values. This choice leads to an optimal match between the histograms (red and black in Figure 7a and b) while keeping the simulation stable.

The PEG-CBT simulations show the same mutual interconnection between the bending and torsion angles as PEG-ReB. The torsion potential, while imposing the desired torsion angle distribution, modifies the bending angle distribution by shifting it to higher bending angle (see the violet curve in Figure 7c and d). This shift can be eliminated by changing the equilibrium bending angle from θ_0 = 130° to θ_0 = 116° (blue curve). In this way, the histograms reproduce the original ones.

Another measure of how the configurations of the polymer chains are affected is the mean square radius of gyration R_g. We find that R_g of the simulated PEG chains remains largely unaffected (see Table 4).

Table 4. Calculated Mean Square Radius of Gyration R_g of PEG Chains in Water and PS Polymer Chains with Different Lengths in Benzene, at T = 300 K[a]

chain	OR	CBT	ReB
PEG37	1.56 ± 0.25	1.47 ± 0.22	1.54 ± 0.24
PS10	0.49 ± 0.06	0.75 ± 0.01	0.74 ± 0.01
PS30	1.53 ± 0.18	1.86 ± 0.01	1.65 ± 0.02
PS60	2.55 ± 0.35	3.29 ± 0.10	2.77 ± 0.06
PS100	3.42 ± 0.56	5.00 ± 0.29	3.79 ± 0.83

[a]The model parameters are given in Tables 3 and 5, respectively.

Polystyrene (PS). In the second study, we have simulated polystyrene (PS) chains in dilute solutions in good solvent (benzene) and as melt. As the starting model, we have used the original coarse-grained MARTINI model of polystyrene (PS) developed by Rossi et al.[23] In this model, named here PS-OR, each PS monomer is described by four coarse-grained beads. As shown in Figure 8, one bead (B) represents the C_α−C_β backbone and three beads (R) represent the phenyl ring (in the same fashion as for the MARTINI representation of benzene). Harmonic bond potentials are used to model the BR and RB bonds and constraints for the RR bonds. Three bending potentials control the angle types BRB, RBR, and BRR. The original topology for bonded interactions did not include any torsional potential. This model reproduces accurately the

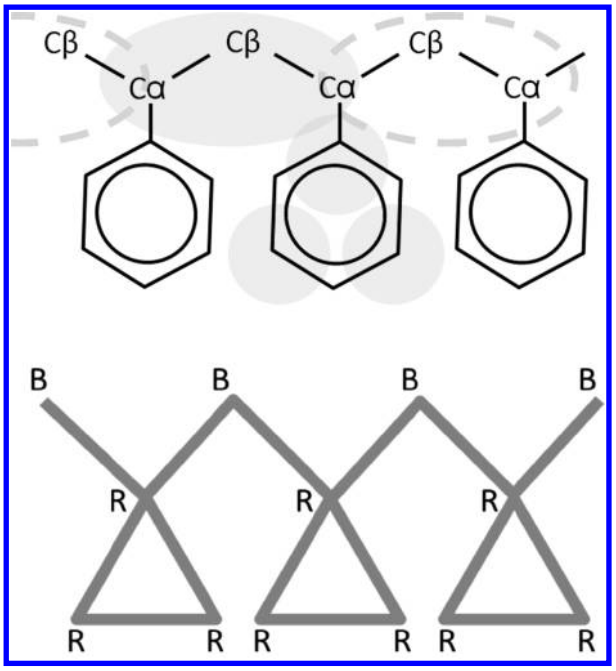

Figure 8. Top: a trimer of PS, in atomistic (black) and CG representation (gray circles). Bottom: the CG representation, where backbone beads are named B and ring beads are named R.

bond and bending angle distributions obtained in simulations at the atomistic level, and it is stable in MD runs with a 20 fs time step. Since it does not include the torsion interactions, it poorly describes the distribution of backbone dihedrals as illustrated in Figure 9. A more accurate treatment of the dihedrals is important to distinguish among the possible different tacticities of polystyrene, one of the conclusions of the original paper.[23] By making use of the newly implemented potentials, we modified the PS-OR model to additionally include the backbone torsion interaction on the BRBR angle. This choice was natural and consistent with the bending angle interactions already considered.

As in the case of PEG, two models are proposed and tested. In the PS-ReB model, we use the ReB potential to describe the BRB and RBR bending angles and a simple Ryckaert–Bellemans function for the dihedral itself. In the PS-CBT model, we couple the backbone torsional degree of freedom to the standard harmonic BRB and RBR angles by means of the CBT potential. All the parameters for the new topologies are gathered in Table 5.

The tuning of the new topology parameters for bonded interactions was based on the reproduction of the atomistic bonded distributions. The distributions obtained using the PS-ReB and PS-CBT models are shown in Figure 9. All distributions were obtained from a coarse-grained simulation of a single PS10 chain in benzene, running with a time step of 20 fs for 3 μs, at T = 300 K (Nose–Hoover thermostat) and P = 1 bar (Parrinello–Rahman barostat). The contributions of free chain ends were discarded. Extensive details about the atomistic force-field used and simulation setup can be found in the original publication.[23]

For further validation, we compared the value of the mean square radius of gyration, R_g, of PS-ReB and PS-CBT in a good solvent, benzene, to that obtained with the original model PS-OR.[24] Simulations consisted of single PS chains (PS10, PS30, PS60 and PS100) in benzene, running with a time step of 20 fs

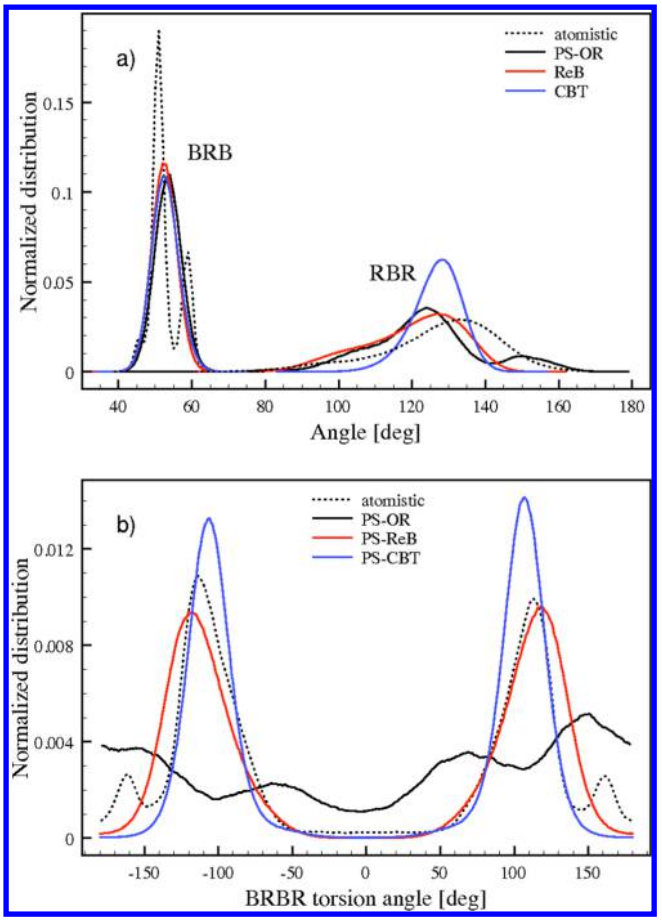

Figure 9. Atomistic and CG distributions of backbone bending and torsion angles in PS.

for 3, 4, 6, and 6 μs, respectively, in the NPT conditions described. The results are shown in Table 4. The addition of the torsion potential increases the chain stiffness, and larger R_g values are obtained for PS chains using both the ReB and CBT models. In consequence, we expect the thermodynamic behavior to be affected (in particular, the increase of the glass transition temperature in polymer melts, as observed by Bulacu and Van der Giessen[25]). A better match with the original model would require further refinement of the nonbonded interaction of the coarse-grained PS beads.

The simulation of a PS melt is a stringent test for the stability of the new models. The large number of dihedral angles in multiple polymer chains and the high temperature used in simulations challenge the numerical stability. We thus performed two simulations of a melt of 18 PS100 chains using both PS-ReB and PS-CBT, at T = 500 K and T = 650 K, with a time step of 20 fs and the usual NPT settings. The PS-ReB model was stable for 1.3 μs at 500 K and only for 6 ns at 650 K. In contrast, the PS-CBT model did not experience any numerical instabilities. Both simulations at T = 500 and 650 K successfully completed a run time of 3 μs.

Coarse-Grained Simulations of Proteins. The different potentials described in the method sections were also tested on their ability to repair the numerical instability of the protein MARTINI backbone in extended or β-sheet secondary structure regions. One should keep in mind that the dihedral potentials tested will in any manner affect the overall description of protein structures by the MARTINI force field.

dx.doi.org/10.1021/ct400219n | J. Chem. Theory Comput. 2013, 9, 3282–3292

Table 5. Angle Potentials Used in the PS Simulations: Type, Reference Angle, and Optimum Interaction Parameters[a]

	BRB			RBR			BRBR	
	type	θ_0 [deg]	k_B [kJ mol^{-1}]	type	θ_0 [deg]	k_B [kJ mol^{-1}]	type	a_i[kJ mol^{-1}]
PS-OR	CH	52	550	CH	120	25		
PS-ReB	ReB	52	25	ReB	120	50	RB	a_0 = 1.0
	CH	52	550					a_1 = −8.0
								a_2 = 2.0
								a_3 = 4.0
								a_4 = 6.0
PS-CBT	CH	60	550	CH	110	250	CBT	k_ϕ = 5.0
								a_0 = 13.0
								a_1 = 8.4
								a_2 = 8.2
								a_3 = −9.1
								a_4 = 0.0

[a]The definition of the bending angles BRB and RBR and torsion angle BRBR is shown in Figure 8b.

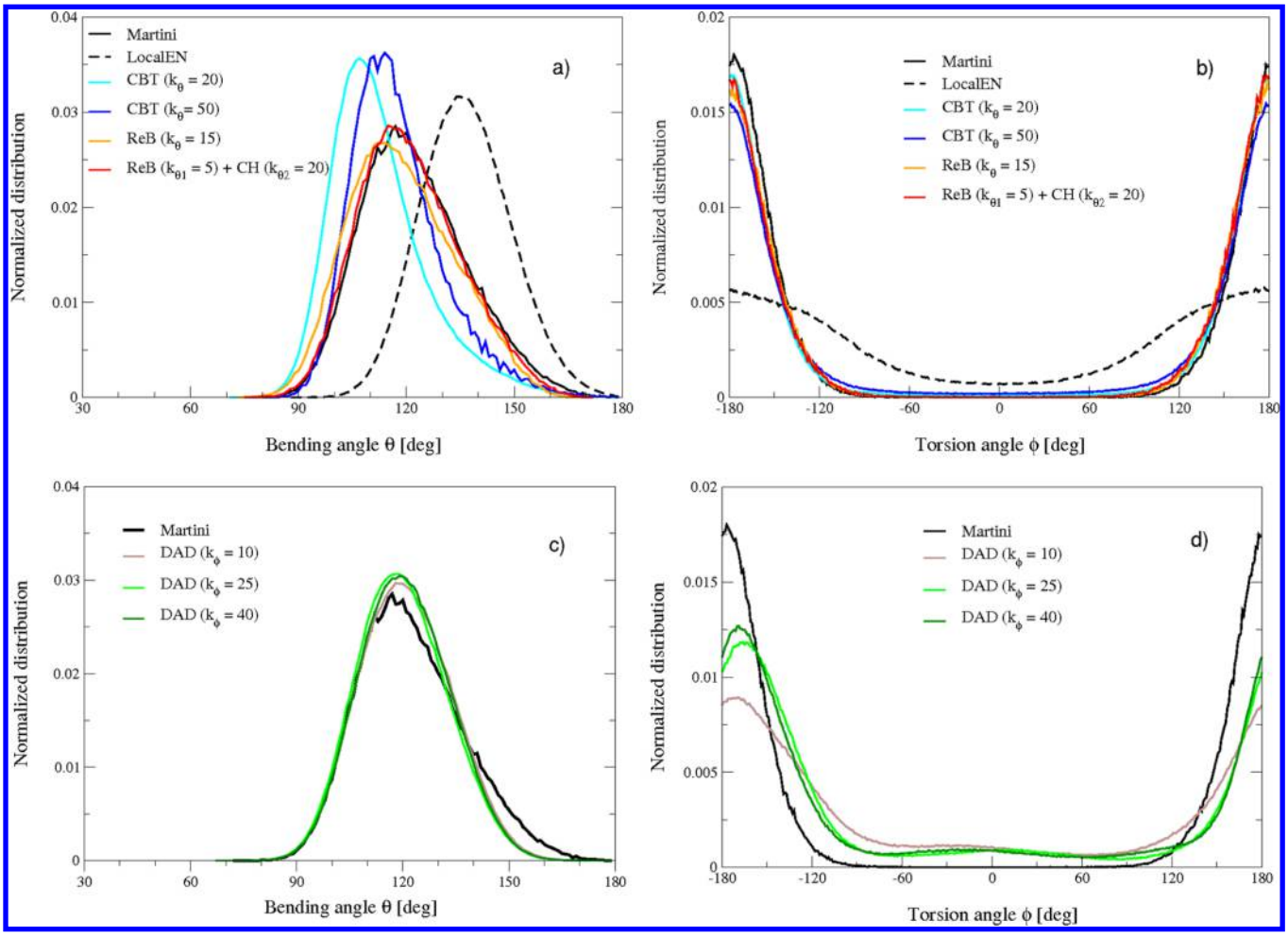

Figure 10. Probability distributions of the bending and torsion angles from the extended secondary structure section of the protein with the PDB entry 1TEN. The bending angles are defined by three consecutive B particles. Histograms obtained with different potentials are shown: (a and b) for the ReB and CBT potentials and (c and d) for DAD. The force constants referred in the figure are given in kJ mol^{-1} units.

In particular, the new potentials will not change the deformation of the β-sheet structures. Briefly, the MARTINI protein force field[19] has inherited the general 4:1 mapping used to define chemical groups as beads and the broad experience in using partitioning data for parametrization. Each amino acid is represented by one bead for the backbone and from zero (Gly and Ala) to four (Trp) beads for the side chain. The bonded terms were extracted from a set of protein structures with the backbone bead placed on the center of mass (COM) of the backbone. Partitioning behavior of side chain analogues were used to determine the nonbonded interactions. The numerical instability of the MARTINI backbone is due to the near alignment of three consecutive backbone beads in an extended conformation. In a first attempt of solving this problem, a local

elastic network (LocalEN) was added to MARTINI: the backbone was replaced by a set of three unnatural bonds between 1−3, 2−4 and 1−4 pairs of atoms, defining the 1234 dihedral.

Here, we used the fibronectin type III domain from tenascin (PDB-ID 1TEN), a β-sheet protein, as a model system. We tested the CBT, ReB, and DAD potentials with some variants and find all the versions but the original MARTINI stable when running with a time step of 20 fs for 10 μs. The original MARTINI model ran with a 10 fs time step. Note that the overall native structure of the protein was not conserved with any of the potentials tested. Typically, the root-mean-square-deviation of the backbone beads reaches a plateau value of 0.6−0.8 nm. This is not a matter for the current study; the MARTINI protein force field is not very good at keeping β-sheets in general. When the native 3D protein structure is of crucial importance in simulations, a global elastic network (ElNeDyn[26]) should be used.

The distributions of the dihedrals and of their associated bending angles, obtained from the first 2 μs simulation, are shown in Figure 10. First, it is clear that the histograms obtained using the LocalEN approach are slightly modified compared to the original MARTINI (see the solid and dashed black curves in Figure 10a and b). The backbone angle distribution is shifted by ≈20 degrees to higher values and the dihedral angles partly lose their originally strong preference for values around 180°, corresponding to an extended structure. Although the reason underlying these deformations is not clear, they can be avoided by using any of the new potential forms described in the methods section.

It is interesting to note that the CBT potential needed some modification of the original backbone angle to reproduce the original distribution, while there was only little effect on the backbone torsion angle. The bending angle force constant was increased from 25 kJ mol^{-1} to 50 kJ mol^{-1} (cyan and blue lines in Figure 10). This result indicates that the CBT potential affects the bond angles associated with it, as in the case of polymers.

We have also tested the use of ReB to replace the conventional cosine potential used in MARTINI to model the bond angles. The ReB was used either to completely replace the cosine potential (orange curves) or in addition to the regular angle to introduce a high-energy penalty when the angle approaches values close to 180° (red curves in Figure 10). Both solutions appeared to be satisfactory since they preserved the original angle and dihedral distributions of the backbone. In the case of already existing parameters using conventional dihedral angles, the ReB might be the most appropriate solution, since it does not require any reparameterization. Its advantage is to provide a steep energy barrier close to angle values close to 180° while it does not affect the original potential on the most relevant range of values explored.

The direct applicability of the DAD potential (no need of code change) was convenient, although it needed some tuning of the backbone torsion angle but not of the bending angle. The DAD potential does not reproduce the exact distribution of the backbone torsion, expected since the motion around the central DD bond is different from the motion around the BB bond. DAD notably seems to allow more flexibility than the other potentials around 180° (Figure 10c and d). This feature might be an intrinsic property of the combination of the DAD potential with the MARTINI backbone since strengthening the torsion potential has only limited effect on the distribution at 180°.

CONCLUSIONS

In this paper, we aim to methodically fix numerical instabilities known to occur in coarse-grained simulations during the calculation of the dihedral potential. Two independent solutions are proposed. The first makes use of novel forms for the angle potentials: the restricted bending (ReB) potential prevents the molecules from visiting unstable or unphysical configurations while the combined bending-torsion (CBT) potential smoothly cancels the interactions when such configurations are sampled. In the second approach—dummy-assisted dihedral (DAD)—the torsion potential is applied differently: instead of acting on real beads, it acts on extra beads added to the real ones. For simple geometrical reasons, in this case, the unstable region is not part of the accessible conformational space.

The stability of the simulations using the new methods has been demonstrated in various simulations of polyethylene glycol (PEG), polystyrene (PS), and polypeptides molecules described by the MARTINI force field. Multiple simulations up to tens of microseconds have been performed using larger simulation time steps and at higher temperatures as compared to the previous procedures. The simulation results have been compared with results from their corresponding atomistic and/or available coarse-grained simulations. Good agreement has been found between the calculated histograms of the bending and torsion angles for both polymers and proteins. The modified potentials are thus effective in avoiding singularities without significantly changing the behavior of the simulated systems.

AUTHOR INFORMATION

Corresponding Author

*E-mail: m.i.bulacu@gmail.com; tieleman@ucalgary.ca; s.j.marrink@rug.nl.

Notes

The authors declare no competing financial interest.

ACKNOWLEDGMENTS

M.B., X.P., and N.G. would like to thank Alex de Vries and Durba Sengupta for helping us during the testing of the methods and David van der Spoel and Berk Hess for their help in implementing the new angle potentials in the next Gromacs release. The National Computing Facilities (The Netherlands) is acknowledged for the use of supercomputer facilities. Part of this work was supported by the Natural Science and Engineering Research Council (Canada). W.Z. was supported by a fellowship from Alberta Innovates Health Solutions. D.P.T. is an Alberta Innovates Health Solutions Scientist and Alberta Innovates Technology Futures Strategic Chair in (Bio) Molecular Simulation.

REFERENCES

(1) Marrink, S. J.; Risselada, H. J.; Yefimov, S.; Tieleman, D. P.; de Vries, A. H. *J. Phys. Chem. B* **2007**, *111*, 7812−7824.
(2) Marrink, S. J.; Tieleman, D. P. *Chem. Soc. Rev.* **2013**, DOI: 10.1039/C3CS60093A.
(3) Schlick, T.; Peskin, C.; Broyde, S.; Overton, M. *J. Comput. Chem.* **1987**, *8*, 1199−1224.
(4) Schlick, T. *J. Comput. Chem.* **1989**, *10*, 951−956.
(5) Moss, G. P. *Pure Appl. Chem.* **1996**, *68*, 2193−2222.

(6) Hess, B.; Kutzner, C.; van der Spoel, D.; Lindahl, E. *J. Chem. Theory Comput.* **2008**, *4*, 435−447.
(7) Humphrey, W.; Dalke, A.; Schulten, K. *J. Mol. Graphics* **1996**, *14*, 33−38.
(8) Ryckaert, J.-P.; Bellemans, A. *Chem. Phys. Lett.* **1975**, *30*, 123−125.
(9) Steele, D. *J. Chem. Soc., Faraday Trans. II* **1985**, *81*, 1077−1083.
(10) Jorgensen, W. L.; Madura, J. D.; Swenson, C. J. *J. Am. Chem. Soc.* **1984**, *106*, 6638−6646.
(11) Bulacu, M.; Van der Giessen, E. *J. Chem. Phys.* **2005**, *123*, 114901.
(12) Bernabei, M.; Moreno, A. J.; Colmenero, J. *Phys. Rev. Lett.* **2008**, *101*, 255701.
(13) Bulacu, M.; Van der Giessen, E. *J. Chem. Phys.* **2009**, *131*, 064904.
(14) Bulacu, M.; Van der Giessen, E. *Europhys. Lett.* **2011**, *93*, 63001.
(15) Solar, M.; Van der Giessen, E. *Comput. Mater. Sci.* **2012**, *64*, 187−191.
(16) Scott, R. A.; Scheraga, H. A. *J. Chem. Phys.* **1966**, *44*, 3054−3069.
(17) Pauling, L. *The Nature of Chemical Bond*; Cornell University Press: Ithaca and New York, 1960; pp 1077−1083.
(18) van Duin, A. C. T.; Dasgupta, S.; Lorant, F.; Goddard, W. A. *J. Phys. Chem. A* **2001**, *105*, 9396−9409.
(19) Monticelli, L.; Kandasamy, S. K.; Periole, X.; Larson, R. G.; Tieleman, D. P.; Marrink, S.-J. *J. Chem. Theory Comput.* **2008**, *4*, 819−834.
(20) de Jong, D. H.; Singh, G.; Bennett, W. F. D.; Arnarez, C.; Wassenaar, T. A.; Schafer, L. V.; Periole, X.; Tieleman, D. P.; Marrink, S. J. *J. Chem. Theory Comput.* **2013**, *9*, 687−697.
(21) Allen, M. P.; Tildesley, D. J. *Computer Simulation of Liquids*; Clarendon Press: Oxford, 1987; pp 329−332.
(22) Lee, H.; de Vries, A. H.; Marrink, S.-J.; Pastor, R. W. *J. Phys. Chem. B* **2009**, *113*, 13186−13194.
(23) Rossi, G.; Monticelli, L.; Puisto, S. R.; Vattulainen, I.; Ala-Nissila, T. *Soft Matter* **2011**, *7*, 698−708.
(24) Rossi, G.; Elliot, T., I. G.; Ala-Nissila; Faller, R. *Macromolecules* **2011**, *45*, 563.
(25) Bulacu, M.; Van der Giessen, E. *Phys. Rev. E* **2007**, *76*, 011807.
(26) Periole, X.; Cavalli, M.; Marrink, S.; Ceruso, M. *J. Chem. Theory Comput.* **2009**, *5*, 2531−2543.